Contribution from the Department of Chemistry,
University of Minnesota, Minneapolis, Minnesota 55455

Excited-State Properties of $[M(COD)(\mu\text{-}L)]_2$ Complexes (M = Rh, Ir; μ-L = Substituted Hydroxypyridinate). Relationship of Variable-Temperature Emission Lifetime and Quantum Yield Measurements to the Photoreduction of Halocarbons

Gary S. Rodman, Charles A. Daws, and Kent R. Mann*

Received November 6, 1987

We measured the electronic absorption and emission properties of $[M(COD)(\mu\text{-}L)]_2$ (M = Rh, Ir; COD = 1,5-cyclooctadiene; μ-L = hp (2-hydroxypyridinate), mhp (6-methyl-2-hydroxypyridinate), chp (6-chloro-2-hydroxypyridinate), 2hq (2-hydroxyquinolate), pz (pyrazolate)) complexes and the deactivation parameters of the ^3B state of $[Ir(COD)(\mu\text{-}L)]_2$ in MTHF (MTHF = 2-methyltetrahydrofuran). Each Rh and Ir complex exhibits an intense absorption band around 420 and 490 nm, respectively, that is assigned to the $^1A \rightarrow {}^1B$ component of the $d\sigma^* \rightarrow p\sigma$ transition. The Ir complexes exhibit temperature-dependent phosphorescence bands ($\lambda_{max} > 720$ nm) and temperature-independent fluorescence bands ($\lambda_{max} \approx 610$ nm). The temperature dependence of the phosphorescence intensity was fit to the following expression: $1/\phi_{obsd} = 1/\phi_0 + A' \exp(-E_a/k_BT)$. For μ-L = hp, $E_a = 2030$ cm^{-1}, $A' = 0.021 \times 10^9$, $\phi_0 = 0.0189$; for μ-L = mhp, $E_a = 2070$ cm^{-1}, $A' = 0.45 \times 10^9$, $\phi_0 = 0.0162$; for μ-L = pz, $E_a = 4467$ cm^{-1}, $A' = 280 \times 10^9$, $\phi_0 = 0.093$. Variable-temperature lifetime data was fit to an analogous equation: $k_{obsd} = k_0 + A \exp(-E_a/k_bT)$. For μ-L = hp, $E_a = 1620$ cm^{-1}, $A = 3.2 \times 10^{12}$ s^{-1}, $k_0 = 1.04 \times 10^6$ s^{-1}; for μ-L = mhp, $E_a = 1950$ cm^{-1}, $A = 5.6 \times 10^{12}$ s^{-1}, $k_0 = 1.11 \times 10$ s^{-1}; for μ-L = chp, $E_a = 1900$ cm^{-1}, $A = 8.0 \times 10^{12}$ s^{-1}, $k_0 = 1.61 \times 10^6$ s^{-1}; for μ-L = hq, $E_a = 1950$ cm^{-1}, $A = 3.4 \times 10^{12}$ s^{-1}, $k_0 = 1.74 \times 10^6$ s^{-1}; for μ-L = pz, $E_a = 3750$ cm^{-1}, $A = 310 \times 10^{12}$ s^{-1}, $k_0 = 0.48 \times 10^6$ s^{-1}. The hydroxypyridinate complexes have shorter intrinsic (temperature-independent) lifetimes and quantum yields than $[Ir(COD)(\mu\text{-}pz)]_2$, but no systematic differences in excited-state properties could be discerned within the hydroxypyridinate series. These results are rationalized on the basis of the "energy gap law" and the Strickler–Berg equation. The thermal deactivation barrier for the ^3B excited state of $[Ir(COD)(\mu\text{-}pz)]_2$ is much larger in MTHF than in acetonitrile. Because of a lower energy ligand field (LF) state, the deactivation barrier in the hydroxypyridinate complexes is significantly smaller than in the pz complex. The differences observed in the photochemical reactivity of $[Ir(COD)(\mu\text{-}hp)]_2$ and $[Ir(COD)(\mu\text{-}pz)]_2$ with halocarbons are rationalized in terms of differences in the rates of reactions that follow electron transfer from the ^3B excited state.

Introduction

In a recent communication,[1] we reported the synthesis and characterization of new binuclear iridium(I) and rhodium(I) hydroxypyridinate complexes of the form $[M(COD)(\mu\text{-}L)]_2$ (M = Rh, Ir; COD = 1,5-cyclooctadiene; L = 2-hydroxypyridinate (hp), 6-methyl-2-hydroxypyridinate (mhp)) that contain the d^8–d^8 chromophore (see Figure 1). The lowest excited state of $[Ir(COD)(\mu\text{-}hp)]_2$ in fluid solutions exhibits emissive behavior and undergoes a formal four-electron oxidation reaction in CCl_4 solutions but is unreactive in CH_2Cl_2. The dramatically lower reactivity of this excited state with CH_2Cl_2 in comparison with the analogous $[Ir(COD)(\mu\text{-}pz)]_2$ (pz = pyrazolate) excited state prompted us to investigate a series of complexes by photophysical methods. The results of variable temperature excited state lifetime and luminescence quantum yield measurements for $[Ir(COD)(\mu\text{-}L)]_2$ (L = hp, mhp, chp, and 2hq; chp = 6-chloro-2-hydroxypyridinate and 2hq = 2-hydroxyquinolate) and $[Rh(COD)(\mu\text{-}mhp)]_2$ enable a comparison of the photophysics and photochemistry of $[Ir(COD)(\mu\text{-}pz)]_2$ and $[Ir(COD)(\mu\text{-}hp)]_2$ to be made. Although the reduction potential of the lowest lying triplet excited state of $[Ir(COD)(\mu\text{-}hp)]_2$ is very similar to that of $[Ir(COD)(\mu\text{-}pz)]_2$, decreases in the rates of steps that follow the transfer of the first electron to the halocarbon may be responsible for the decrease in the excited-state reactivity of the hp complexes.

Experimental Section

Sample Preparation. The preparation of the hydroxypyridinate complexes has been previously reported.[1,2] $[Ru(bpy)_3][Cl]_2$ was obtained from Aldrich. The solvent 2-methyltetrahydrofuran (MTHF) was twice distilled from sodium benzophenone ketyl and stored over sodium metal under vacuum. Spectral grade toluene was stored over P_4O_{10} under vacuum. Samples used for spectral and 77 K quantum yield measurements were prepared as follows: Solids were placed in 1-cm square Pyrex cuvettes equipped with ground-glass joints and high-vacuum stopcocks. Degassed (four freeze–pump–thaw cycles) MTHF was vacuum transferred into the evacuated cuvettes, which were then sealed with a torch. For variable-temperature emission lifetime and quantum yield studies, round Pyrex tubes 1 cm in diameter were used as sample cells. Samples were prepared as above.

Absorption and Emission Spectra. Emission spectra were recorded on a Spex 112X spectrofluorometer operated in ratio mode. Emission from solution samples was detected normal to the incident light. Spectra reported here are corrected for monochrometer and photomultiplier response. Absorption spectra were obtained on a Cary 17D spectrophotometer interfaced to a Zenith 150 microcomputer.

Emission Lifetimes. Samples were excited at 532 nm with the frequency doubled output of a Molectron Nd:YAG laser (pulse width = ca. 20 ns; pulse rate = 10 hz). Emission was detected normal to the excitation beam by using a PMR Optics MCI-02 monochromator (slits = 0.6 mm) attached to an EMI 9785B photomultiplier tube. Stray laser light was removed with a 560-nm glass cutoff filter positioned between sample and monochromator. The PMT signal was amplified with a Pacific Precision Instruments 2A44 video amplifier and digitized with a Data Precision Model 6000 transient digitizer equipped with the Model 620 digitizing plug-in.

Data was transferred to a Zenith 150 microcomputer for storage and analysis. Each lifetime determination was a signal average of at least 100 wave forms. Three determinations were made at each temperature and the results averaged. The intensity vs time data was fit to a simple first-order kinetic decay scheme to give the observed emission lifetime τ_{obsd}. Plots of ln $(I(t))$ vs t were linear for at least 3 half-lives. The temperature dependent lifetimes were fit to the three-parameter model shown in eq 1, where τ_{obsd} = the observed lifetime, k_0 = low-temperature

$$1/\tau_{obsd} = k_{obsd} = k_0 + A \exp(-E_a/k_BT) \quad (1)$$

limiting deactivation rate, and A and E_a are the Arrhenius activation parameters for the temperature-dependent deactivation process, and k_B is the Boltzman constant (see Appendix).[33]

Phosphorescence Quantum Yields. Phosphorescence quantum yields of the Ir_2 compounds were determined at 77 K in MTHF glasses by using the comparative method outlined by Demas and Crosby.[3] $Ru(bpy)_3^{2+}$ in water at 298 K was used as the standard ($\phi = 0.042$).[4] $Ru(bpy)_3^{2+}$ solutions were prepared with the same absorbance as the Ir_2 samples at the excitation wavelength at 77 K. The standard solutions were bubble degassed with O_2-scrubbed nitrogen for 20 min. Equation 2 was used

$$\phi_s = 0.042(f_r/f_s)(I_s/I_r)(n_s^2/n_r^2) \quad (2)$$

to calculate the phosphorescence quantum yields, ϕ_s. In eq 2, f refers to the fraction of light absorbed at the excitation wavelength, I to the

* To whom correspondence should be addressed.

(1) Rodman, G. S.; Mann, K. R. *Inorg. Chem.* **1985**, *24*, 3507.
(2) Rodman, G. S.; Mann, K. R. *Inorg. Chem.*, in press.
(3) Demas, J. N.; Crosby, G. A. *J. Am. Chem. Soc.* **1971**, *75*, 991.
(4) Van Houton, J.; Watts, R. J. *J. Am. Chem. Soc.* **1976**, *98*, 4853.

0020-1669/88/1327-3347$01.50/0

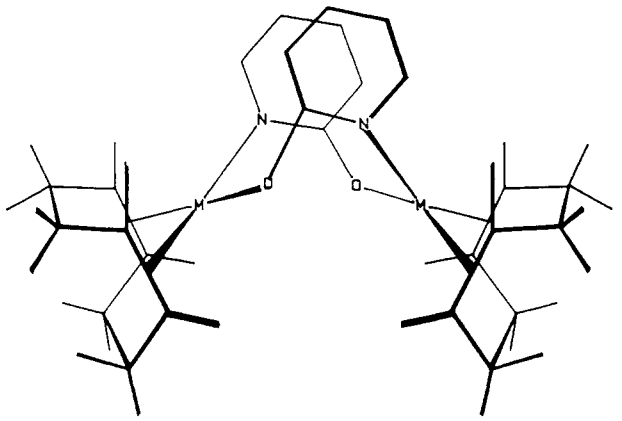

Figure 1. Structure of $[M(COD)(\mu\text{-hp})]_2$ binuclear complex.

integrated intensity of the emission band plotted on an energy scale, and n to the refractive index of the solvent. The subscripts s and r refer to Ir_2 sample and Ru reference solutions, respectively. The value for the refractive index of MTHF at 77 K was estimated by using eq 3,[5] which

$$(n^2 - 1)/(n^2 + 2) = K_{solv}d \qquad (3)$$

relates the refractive index of a solvent to its density, d. K_{solv} is a collection of temperature-independent constants, including solvent molecular weight, polarizability, and permanent dipole moment. The density of MTHF at various temperatures was determined as described below.

The phosphorescence quantum yields at temperatures other than 77 K were calculated relative to the 77 K values by using eq 4, where $I(T)$

$$\phi(T) = \phi(77\text{ K})\left[\frac{(I(T))(n(T))}{(I(77\text{ K}))(n(77\text{ K}))}\right] \qquad (4)$$

refers to the integrated emission intensity at temperature T corrected for the changes in the fraction of exciting light absorbed as the temperature was varied. The refractive index of MTHF at temperature T was determined from eq 3. The absorption correction factors were generated from separate studies of the temperature dependence in the absorption spectra of the Ir_2 compounds, described below. Excitation was ca. 20 nm to higher energy of the d–p absorption maximum in each compound.

The temperature-dependent quantum yields were fit to the model in eq 5, where ϕ_0 is the low-temperature limit of the observed quantum

$$1/\phi_{obsd} = 1/\phi_0 + A'\exp(-E_a/k_BT) \qquad (5)$$

yields (above the glass transition region), k_B is the Boltzman constant, and A' and E_a are the Arrhenius parameters for deactivating the ^3B excited state. A' is related to the A factor derived from the lifetime measurements by $A' = A/(\phi_{isc}k_r)$ (see Appendix[33]).

Variable-Temperature Measurements. Measurements at 77 K were carried out with locally constructed optical Dewars filled with liquid nitrogen. Variable-temperature measurements were obtained with an Air Products Model 202 Displex cryostat. A thermocouple (chromel vs gold 0.0m% iron) and resistance heater were bonded to the cold tip of the cryostat. Temperatures were set and maintained with an Air Products Model APD-E temperature indicator/controller. The temperature controller was calibrated at liquid-N_2 and water/ice temperatures. Temperatures are estimated to be reproducible to within 2 K. Sealed sample cells were placed in a locally constructed copper sample holder with windows cut to allow for 90 or 180° monitoring relative to the incident radiation. Cry-Con conductive grease was used to increase the thermal contact between sample and cell holder. Samples were allowed to reach thermal equilibrium with the cold tip by waiting at least 15 min at each temperature before data collection.

Spectra obtained at different temperatures were corrected for changes in sample density by measuring the change in volume of a fixed amount of solvent. This was accomplished by adding ca. 0.5 mL of the appropriate solvent to a 1-mL volumetric pipet (0.01-mL divisions, sealed at one end with a torch. The dead volume between the lowermost calibration and the bottom of the pipet was measured by repeated fillings with a 100 μL syringe. The solvent was frozen and the tube evacuated; the top of the pipet was then sealed off with a torch. The pipet was then immersed in a Dewar containing baths of known temperatures. Volumes could be estimated to ±0.001 mL. Contraction factors were then generated from plots of volume vs temperature.

(5) Suppan, P.; Tsiamis, C. *J. Chem. Soc., Faraday Trans. 2* **1981**, 1553.

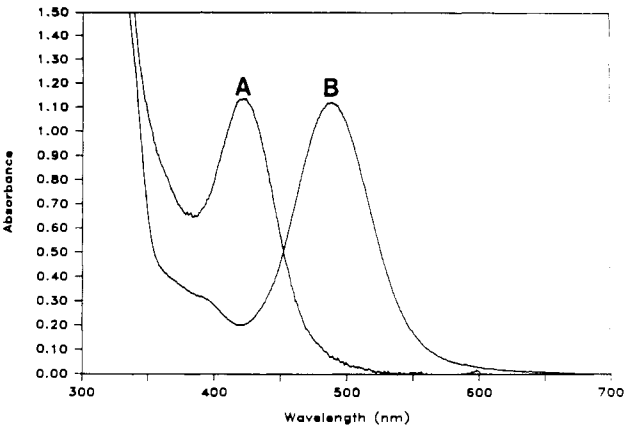

Figure 2. 295 K absorption spectra of $[Rh(COD)(\mu\text{-mhp})]_2$ in MTHF (curve A) and $[IrnCOD)(\mu\text{-hp})]_2$ in MTHF curve B).

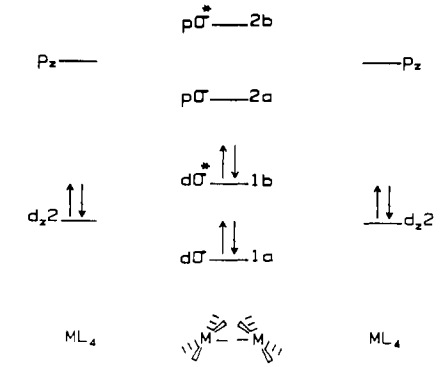

Figure 3. Qualitative molecular orbital diagram for d^8–d^8 binuclear complexes with C_2 symmetry.

Table I. Electronic Absorption Parameters for $[M(COD)(\mu\text{-L})]_2$ in MTHF at 295 K

M	μ-L	λ_{max}, nm	ϵ_{max}, M^{-1} cm^{-1}	λ_{max}, nm	ϵ_{max}, M^{-1} cm^{-1}
Ir	hp	490	4700	599	190
	mhp	484	4600	575	360
	chp	490	5100	586	130
	2hq	499	3200	580	290
	pz	499	9100[a]	585	460[a]
Rh	hp	422	3000	482	300
	mhp	420	2800	*b*	*b*
	pz[c]	443	8110	*d*	*d*

[a] Reference 7. [b] Band not observed. [c] THF solution.[7] [d] Values not reported.

Results and Discussion

Electronic Spectra. The 295 K visible absorption spectra of $[Ir(COD)(\mu\text{-hp})]_2$, and $[Rh(COD)(\mu\text{-hp})]_2$, are shown in Figure 2. The positions of the visible absorption bands of the other hydroxypyridinate complexes studied in MTHF are compiled in Table I. Included for comparison are the data for the corresponding $[M(COD)(\mu\text{-pz})]_2$ complexes. In these complexes, the bands occur at about 490 mm for M = Ir and 3300 cm^{-1} higher in energy (430 nm) for M = Rh. Weaker absorptions are observed as shoulders on the low-energy tails of the intense visible bands. Higher energy absorption bands are also observed, but they are not addressed in this study.

The low-energy bands the $[M(COD)(\mu\text{-L})]_2$ complexes display in their electronic absorption spectra are similar to those seen in other d^8–d^8 systems. These bands have been previously assigned to primarily metal-centered $d\sigma^* \rightarrow p\sigma$ abbreviated d–p) transitions, in accordance with the simplified MO scheme proposed by Mann et al.[6] A molecular orbital diagram for the hydroxypyridinate compounds, which belong to the C_2 point group, is shown in Figure

(6) Mann, K. R.; Gordon, J. G., II; Gray, H. B. *J. Am. Chem. Soc.* **1975**, *97*, 3553.

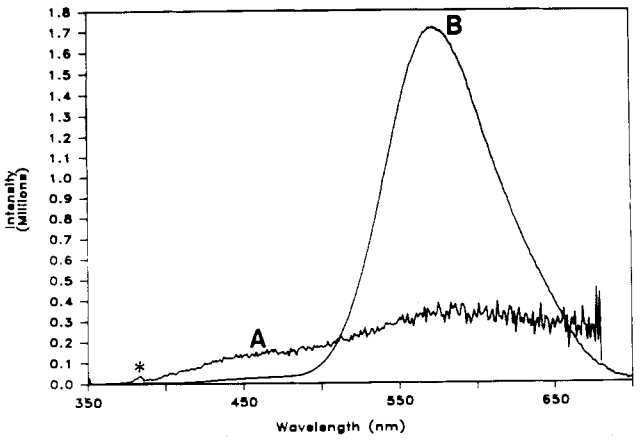

Figure 4. 295 (curve A) and 77 K (curve B) emission spectra of [Ir(COD)(μ-mhp)]$_2$ in MTHF. The asterisk indicates a Raman band of the solvent. The 295 K spectrum was multiplied by a factor of 200.

3. Our axis system is consistent with previous[7] treatments of bent d^8–d^8 systems. The more intense band, which falls between 480 and 500 nm, is assigned as $^1A \rightarrow {}^1B$, $^1(1b)^2 \rightarrow {}^1(1b)^1(2a)^1$, and the weaker, lower energy band, which occurs between 580 and 600 nm, is assigned as $^1A \rightarrow {}^3B$ ($^1(1b^2) \rightarrow {}^3(1b^12a^1)$). The weaker absorption is assigned to the spin-forbidden d → p transition rather than to a spin-allowed d–d band, because the 3000-cm^{-1} energy difference between the weak and strong absorption maxima in each complex is about the same as that between the two observed emission bands (vide infra).

Previous work[8] has shown that in "face-to-face" (D_{4h} or D_{2d}) molecules the energy of the d–p transition is correlated to the metal–metal distance, with shorter distances yielding lower energy absorptions. This effect is observed in the "open-book" complexes considered here as well. The crystal structure of [Ir(COD)(μ-mhp)]$_2$ (λ_{max} = 484 nm) gives an Ir–Ir distance of 3.242 (1) Å, 0.026 Å longer than that of [Ir(COD)(μ-pz)]$_2$ (λ_{max} = 498 nm). Perhaps the slight differences observed in the absorption maxima within the hydroxypyridinate series reflect small variations in the M–M distances. The complex containing 2hq, the most sterically demanding of the hydroxypyridinate ligands used in this study, has the lowest energy d–p transition. Our findings are consistent with those of Bushnell et al.[9] for a series of substituted pyrazolyl-bridged complexes. These compounds have shorter M–M distances to relieve steric crowding between the bridging ligand substituents and the COD group relative to the parent complex. The shorter M–M distance results in a lower energy absorption band.

The replacement of Ir by Rh has a greater effect on the energy of the d–p transition than hp ring substitution, with the hydroxypyridinate-bridged Rh complex absorptions at ca. 3300 cm^{-1} higher energy than those of their Ir$_2$ analogues. This blue shift is consistent with a decrease in the M–M interaction in the Rh$_2$ systems. The molecular orbital diagram shown in Figure 3 illustrates that a decrease in the M–M interaction decreases the splitting between the bonding and antibonding (a and b) orbitals and leads to an increase in the energy difference between the dσ* (1b) and pσ (2a) orbitals. Further weakening of the M–M interaction by decreasing orbital overlap is predicted to produce a lengthened M–M distance, as is observed in the crystal structures of [Rh(COD)(μ-mhp)]$_2$ and [Ir(COD)(μ-mhp)]$_2$. The M–M distance in [Rh(COD)(μ-mhp)]$_2$ is 0.125 Å longer than that of its Ir$_2$ counterpart. This observation parallels that of the [M(COD)(μ-pz)]$_2$ system, where the M–M distance in [Rh(COD)(μ-pz)]$_2$ is 0.051 Å longer than that of its Ir$_2$ analogue. In the pz systems, the d–p transition is shifted to higher energy, but by a lesser amount, 2500 cm^{-1}. We suggest that the larger *differences* observed for electronic and structural parameters upon metal change within the hydroxypyridinate system are the result of the greater degree of structural flexibility afforded by the eight-membered bridging function present in the hydroxypyridinate complexes. In the pz complexes, the bridging ligands dictate the M–M distance, while in the hydroxypyridinate complexes, electronic factors at the metal are important and result in differences between the Rh and Ir analogues.

Table II. Emission Maxima of [Ir(COD)(μ-L)]$_2$ in MTHF

L	λ_{max}, nm			
	T = 298 K		T = 77 K	
hp	612	738	609	726
mhp	615	733	602	725
chp	622	743	606	738
2hq	*a*	*a*	*a*	737
pz	560	685	546	676

[a] Band not observed.

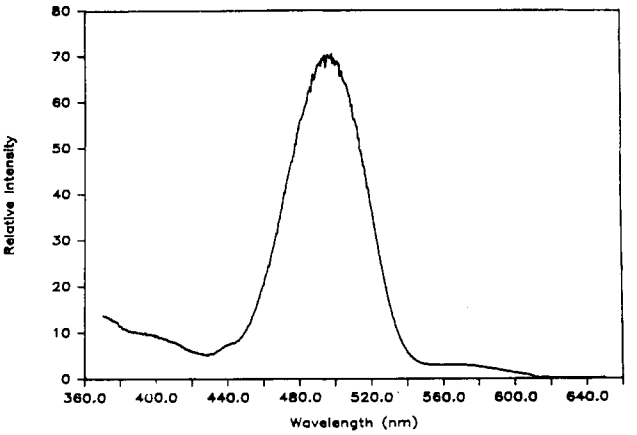

Figure 5. 77 K excitation spectrum of [Ir(COD)(μ-hp)]$_2$ in MTHF. The emission was observed at 690 nm.

Emission and Excitation Spectra. Room-temperature excitation of the d–p transition in [Ir(COD)(μ-L)]$_2$ gives two broad structureless emission maxima between 600 and 750 nm. Figure 4A shows the room-temperature emission spectrum of [Ir(COD)(μ-mhp)]$_2$, which is very similar to that of the hp and chp complexes. The emission of the 2hq complex is difficult to observe at room temperature in fluid solution. Figure 4B shows the 77 K emission spectra of [Ir(COD)(μ-mhp)]$_2$. The emission maxima for all the compounds studied are listed in Table II. For comparison, the emission parameters for [Ir(COD)(μ-pz)]$_2$ are included as well. The lower energy emission band is assigned to the triplet (dσ*pσ) (^3B) → ^1A transition, and the higher energy bands are assigned to the corresponding single (^1B) → ^1A transition. The emission intensity of the triplet state of all four compounds increases dramatically as the temperature is lowered, while that of the singlet state remains essentially constant.

Figure 5 shows the 77 K excitation spectrum of [Ir(COD)(μ-hp)]$_2$. The corrected excitation spectra for all of the of [Ir(COD)(μ-L)]$_2$ complexes at 77 K are very similar to the 77 K absorption spectra, consistent with rapid internal conversion of high-energy excited state to one low-lying singlet and one low-lying triplet excited state, from which emission occurs.

Variable-Temperature Quantum Yields and Phosphorescence Lifetimes. The lifetime of the ^3B state in the [Ir(COD)(μ-L)]$_2$ complexes increases dramatically between room temperature and 77 K. At 295 K, the lifetimes of both the singlet and triplet states were too short to measure on our equipment (detection limit = ca. 70 ns). However at 77 K, the triplet lifetime increased to 1.04 μs for L = hp, with comparable lifetimes for L = mhp and chp. The 2hq complex was shorter lived, with a triplet lifetime of 0.65 μs. These lifetime data are given in Table III, along with the triplet lifetime of [Ir(COD)(μ-pz)]$_2$ in acetonitrile.[7] The ^1B excited-state lifetimes were too short to measure at all temperatures (T > 15

(7) Marshall, J. L.; Stobart, S. R.; Gray, H. B. *J. Am. Chem. Soc.* **1984**, *106*, 3027.
(8) Mann, K. R.; Thich, J. A.; Bell, R. A.; Coyle, C. L.; Gray, H. B. *Inorg. Chem.* **1980**, *19*, 2462.
(9) Bushnell, G. W.; Fjeldsted, D. O. K.; Stobart, S. R.; Zaworotko, M. J.; Knox, S.; MacPherson, K. A. *Organometallics* **1985**, *4*, 1107.

Table III. Excited-State Parameters for $[Ir(COD)(\mu\text{-}L)]_2$ from Lifetime Measurements

L	$10^{-6}k_0$, s^{-2}	$10^{-12}A$, s^{-1}	E_a, cm^{-1}	τ(77 K), μs	τ(295 K), μs
hp	1.04 ± 0.05	3.2 ± 1.0	1620 ± 40	1.04	<0.07
mhp	1.11 ± 0.05	5.6 ± 3.0	1950 ± 70	1.07	<0.07
chp	1.61 ± 0.05	8.0 ± 2.0	1900 ± 60	0.98	<0.07
2hq	1.74 ± 0.05	3.4 ± 0.9	1950 ± 60	0.98	<0.07
pz	0.48 ± 0.07	310 ± 70	3750 ± 40	2.68	<0.25
pz[a]	0.460	1.1	2600	2.51	0.248

[a] Activation energy in acetonitrile reported in ref 7. A factor calculated from 295 K lifetime. k_0 estimated from Arrhenius plot.

Table IV. Excited-State Parameters for $[Ir(COD)(\mu\text{-}L)]_2$ from Emission Measurements

L	E_a, cm^{-1}	$A'10^9$	ϕ_0	ϕ(77 K)	ϕ(295 K)
hp	2030 (10)	0.021	0.025	0.033	2.2×10^{-5}
mhp	2070 (30)	0.45	0.0161	0.034	5.3×10^{-5}
pz	4467 (30)	280	0.093	0.23	8.8×10^{-3}

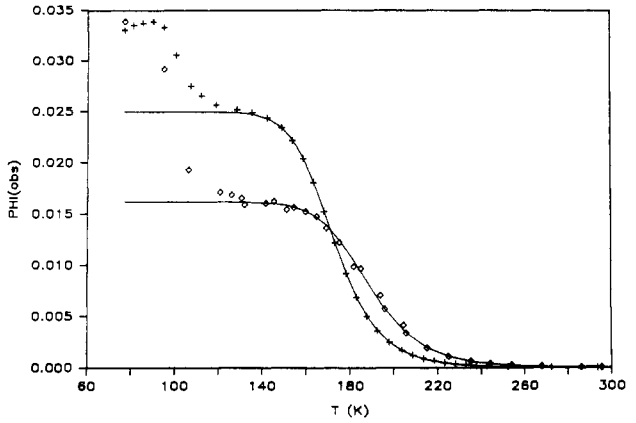

Figure 6. Plot of ϕ_{obsd} vs T for the ^3B exited states of $[Ir(COD)(mhp)]_2$ (+) and $[Ir(COD)(mhp)]_2$ (◆) in MTHF. The solid line is a theoretical plot of ϕ_{obsd} vs T for $\phi_{obsd} = 1/(1 = \phi_0 A' \exp(-E_a/k_B T))$ with values of ϕ_0, E_a, and A' from Table III.

K) on our apparatus. Application of the Strickler–Berg[10] equation to the singlet absorption and emission bands of the hydroxypyridinate complexes predicts a singlet radiative lifetime of 2 ps in accord with lifetime measurements of $[Ir(COD)(\mu\text{-}pz)]_2$, which has a singlet lifetime of less than 20 ps at room temperature.[11] The triplet (phosphorescence) quantum yields of $[Ir(COD)(\mu\text{-}hp)]_2$ and $[Ir(COD)(\mu\text{-}mhp)]_2$ were measured at 77 K and are 0.033 and 0.034, respectively. The 295 K phosphorescence quantum yield of $[Ir(COD)(\mu\text{-}pz)]_2$ was measured in MTHF and was found to be 0.0088, in excellent agreement with the reported value of 0.0078 in acetonitrile.[7] These values are accurate to ±50%, ut their relative precision is much better. The quantum yields at 77 and 295 K for the Ir_2 complexes are compiled in Table IV.

Figure 6 shows plots of the emission quantum yield vs temperature for $[Ir(COD)(\mu\text{-}hp)]_2$ and $[Ir(COD)(\mu\text{-}mhp)]_2$, and Figure 7 shows a similar plot for $[Ir(COD)(\mu\text{-}pz)]_2$. For the hydroxypyridinate complexes, a strongly temperature dependent region is observed between 295 and 140 K. Between 140 and 120 K, the quantum yields are essentially independent of temperature. The large increase in quantum yields between 120 and 77 K corresponds to the glass transition region of MTHF[12] and is due to an increase in the rigidity of the compounds' environment.[13] The behavior of the pz complex is similar, but the onset of the temperature-independent region occurs at a much higher temperature, ca. 240 K.

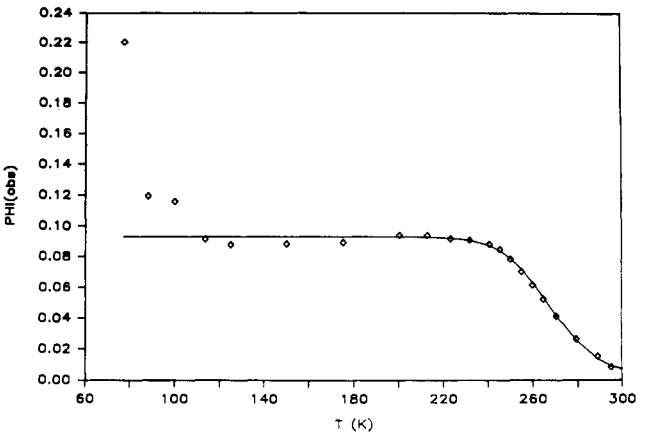

Figure 7. Plot of ϕ_{obsd} vs T for the ^3B excited state of $[Ir(COD)(\mu\text{-}pz)]_2$ in MTHF. The solid line is a plot of ϕ vs T for $\phi_{obsd} = 1/(1 + \phi_0 A' \exp(-E_a/k_B T))$ with value of ϕ_0, E_a and A' from Table III.

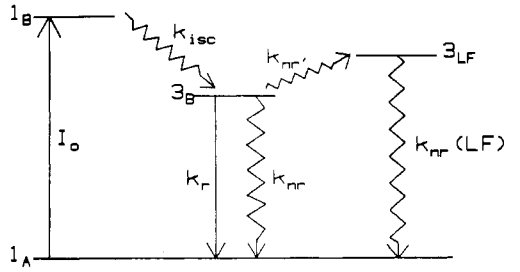

Figure 8. Excited-state energy diagram for $[M(COD)(\mu\text{-}L)]_2$ binuclear complexes. Symmetry labels are those appropriate for the C_2 point group. k_{isc} is assumed to be large ($\phi_{isc} \approx 1$), and deactivation from ^1B to ^1A is ignored. Nonradiative deactivation of ^3LF to $^1A_1$ is assumed to be rapid.

The temperature dependence is caused by a thermally induced deactivation of the lowest triplet excited state (^3B), similar to those observed in other d^8–d^8 systems.[14] The data between 140 and 295 K are fit empirically to eq 5. Equation 5 (derived in the Appendix[33]) is based on the Jablonski diagram shown in Figure 8. The parameter ϕ_0 is the limiting quantum yield above the glass transition region.[15,16] Below the temperature at which ϕ_0 is reached, the thermal deactivation step is not competitive with other deactivation processes. The observed triplet emission quantum yield is defined as

$$\phi_{obsd} = \phi_{isc} \frac{k_r}{k_r + \sum k_{nr}} \tag{6}$$

where k_r is the temperature independent radiative rate constant and $\sum k_{nr}$ is the sum of the nonradiative rate constants. With the assumptions that ϕ_{isc} (the intersystem crossing quantum yield) is independent of temperature and approximately 1, we have

$$\phi_{obsd} = \frac{k_r}{k_r + \sum k_{nr}} \tag{7}$$

Winkler et al.[11] has recently demonstrated that the quantum yield of intersystem crossing is near unity for $[Ir(COD)(\mu\text{-}pz)]_2$. Because the *limiting* quantum yields are less than one, $\sum k_{nr}$ must

(10) Strickler, S. J.; Berg, R. A. *J. Chem. Phys.* **1962**, *37*, 814.
(11) Winkler, J. R.; Marshal, J. L.; Netzel, T. L.; Gray, H. B. *J. Am. Chem. Soc.* **1986**, *108*, 2263.
(12) Ling, A. C.; Willard, J. E. *J. Phys. Chem.* **1968**, *72*, 1918.
(13) Turro, N. J. *Modern Molecular Photochemistry*, Benjamin/Cummings: Menlo Park, NJ, 1978.
(14) Rice, S. F.; Milder, S. J.; Gray, H. B.; Goldbeck, R. A.; Kliger, D. S. *Coord. Chem. Rev.* **1982**, *43*, 349.
(15) The large increases in phosphorescence quantum yields observed in the glass transition region are not consistent with the increases in observed lifetime in the same temperature regime. Between 120 and 77 K, the quantum yields increase by factors of 1.3 and 2.0 for the hp and mhp complexes, respectively. Over the same region, the lifetime increases are 1.1 and 1.2. In this temperature range, k_r increases faster than k_{nr} because, in this regime, $\phi_{obsd} = k_r/(k_r + k_{nr})$ v $k_r \tau_{obsd}$. Other groups[16] have observed anomalies in photophysical parameters in the glass transition region.
(16) Barigelletti, F.; Juris, A.; Balzani, V.; Belsea, B.; Von Zelewsky, A. *Inorg. Chem.* **1983**, *22*, 3335.

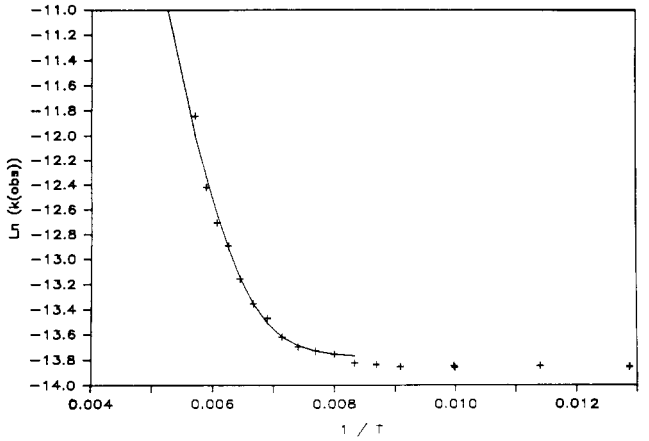

Figure 9. Plot of ln $(1/\tau_{obsd})$ = ln (k_{obsd}) vs $1/T$ for the ^{3}B excited state of [Ir(COD)(μ-hp)]$_2$ in MTHF. + are the experimental points; the solid line is the theoretical line drawn according to eq 1 with k_0, A, and E_a values from Table IV.

include at least two nonradiative pathways, one of which is independent of temperature. Thus, $\sum k_{nr} = k_{nr} + k_{nr'}$. At temperatures low enough to shut off the thermal deactivation process ($k_{nr'}$), most of the excited-state energy (>96% at 77 K) is still lost nonradiatively, through the temperature-independent nonradiative process.

The thermal deactivation term, $A' \exp(-E_a/k_bT)$, in empirical eq 5 corresponds to the nonradiative decay rate constant, $k_{nr'}$ (or $A \exp(-E_a/k_bT)$ divided by k_r). A' is the Arrhenius preexponential A factor divided by k_r. E_a is the Arrhenius activation energy for $k_{nr'}$. Values of the activation parameters A' and E_a calculated from the quantum yield data are listed in Table IV.

Excited-state lifetime measurements are in accord with the quantum yield measurements. Figure 9 presents a plot of ln $(1/\tau_{obsd})$ = ln (k_{obsd}) vs $1/T$ for the ^{3}B state of the representative complex [Ir(COD)(μ-hp)]$_2$. For each complex, we observe a strongly temperature-dependent region above 140 K, but only a slight temperature dependence between 140 and 77 K. Our lifetime data are consistent with the temperature dependence of the phosphorescence quantum yields. The lifetimes vs temperature data were fit to eq 1, appropriate for the model shown in Figure 8.

$$1/\tau_{obsd} = k_{obsd} = k_0 + A \exp(-E_a/k_bT)$$

The data below 120 K were not fit, due to complications that arise from the solvent–glass transition. The rate constant k_0 is the low-temperature limit for k_{obsd} above the glass transition region. It is equal to the sum of the temperature-independent deactivation rates k_r and k_{nr} because at low temperatures the exponential term in eq 1 is negligible. At higher temperatures, the observed decay rate constant, k_{obsd} (the reciprocal of the observed lifetime) is equal to $k_0 + k_{nr'}$. Table III lists the Arrhenius parameters for deactivation of the ^{3}B state of the Ir$_2$ complexes calculated from our lifetime measurements. The quantum yield and lifetime data both allow the activation energy for the nonradiative deactivation pathway to be calculated.

The activation energies calculated for [Ir(COD)(μ-mhp)]$_2$ by the two different methods are in good agreement. The comparable results are less consistent for [Ir(COD)(μ-hp)]$_2$, but we consider the ca. 400-cm^{-1} difference in the calculated activation energies to be the result of our curve-fitting procedure.

Although the dependence of the lifetime of the $^3(d\sigma^*p\sigma)$ ($^3B_2$) state on temperature for [Ir(COD)(μ-pz)]$_2$ in acetonitrile has been studied,[7] the Arrhenius parameters A and E_a are often solvent-dependent, even when the temperature-dependent deactivation process is the same in all environments.[17] To enable further comparisons of the activation parameters of the hydroxypyridinate-bridged compounds to those of [Ir(COD)(μ-pz)]$_2$, it was necessary to reinvestigate the temperature dependence of [Ir(COD)(μ-pz)]$_2$ and to study the excited states in a common solvent. As the hydroxypyridinate complexes are only sparingly soluble in acetonitrile, the pz complex was studied in MTHF. As anticipated, the activation energy is quite solvent-dependent, with an increase from 2600 cm^{-1} in acetonitrile to 3750 cm^{-1} in MTHF. In MTHF, the activation barrier for temperature-dependent, nonradiative deactivation of $^3(d\sigma^*p\sigma)$ is more than twice as large for the pyrazolyl complexes, and the calculated A factor is about 2 orders of magnitude larger.

(17) Milder, S. J. *Inorg. Chem.* **1985**, *24*, 3376.

Table V. Temperature-Independent Deactivation Rate Constants of [Ir(COD)(μ-L)]$_2$ in MTHF

L	k_r,[a] s^{-1}	k_{nr},[b] s^{-1}
hp	2.6×10^4	1.0×10^6
mhp	1.8×10^4	1.1×10^6
pz	4.5×10^4	4.4×10^5

[a] Calculated from $k_r = k_0\phi_0$. [b] Calculated from $k_{nr} = (1 - \phi_0)k_0$.

Table VI. Stokes Shifts of [Ir(COD)(μ-L)]$_2$

compd	Stokes shift, cm^{-1}	compd	Stokes shift, cm^{-1}
[Ir(COD)(μ-hp)]$_2$	4070	[Ir(COD)(μ-chp)]$_2$	4330
[Ir(COD)(μ-mhp)]$_2$	4400	[Ir(COD)(μ-pz)]$_2$	2220

The temperature-independent rate constants k_r and k_{nr}, which are intrinsic parameters of the emitting and ground state, are evaluated by combining the lifetime and quantum yield results (Appendix[33]). The rate constant k_r is calculated from the relation $k_r = k_0\phi_0$, while k_{nr} is calculated from $k_{nr} = k_0(1 - \phi_0)$. These derived values are compiled in Table V and will be discussed below.

Hydroxypyridinate- vs Pyrazolyl-Bridged Complexes. Comparison of Excited-State Structures. With the measured ground- and excited-state parameters for the hydroxypyridinate and pyrazolyl complexes in hand, we can comment on the differences in the excited-state structures of the two types of compounds.

The energy of the d–p absorption band in both types of complexes is about the same, but the energies of both singlet and triplet emissions of the hydroxypyridinate complexes are significantly lower in energy. We interpret the larger Stokes shifts (determined from the difference between absorption and singlet emission maxima, Table VI) observed for the hydroxypyridinate complexes in terms of a larger distortion in the hydroxypyridinate excited-state geometry relative to the ground state. The MO diagram and experimental studies of d^8–d^8 complexes predict a contraction of the M–M distance in flexible complexes upon promotion of an electron into the pσ (2a) orbital because the formal bond order increases from zero to one.[18] A substantial decrease (~0.1 Å) in M–M bond length would be accompanied by other structural changes, such as a decrease in the dihedral angle between the metal coordination planes or an increase in the twist angle. In the lowest triplet state of [Ir(COD)(μ-pz)]$_2$, a rigid system, relatively small distortions from the ground-state geometry are expected for an increase in the M–M bond order. For example,[19] two-electron oxidation of the pz-bridged compound by I$_2$ and MeI (formal removal of two electrons from the 1b orbital and increase of the bond order to one) gives Ir(II)–Ir(II) species with M–M distances of 3.085 and 3.112 Å, respectively, distances only slightly shorter than the 3.216 Å observed in the parent pyrazolyl complex. In the two oxidized complexes, the overall geometry, including the interplanar dihedral angle, was not significantly altered. The COD ligands remained in the sterically less favorable eclipsed conformation. Oxidation of the less sterically hindered complex [Ir(CO)(PPh$_3$)(μ-pz)]$_2$[20] by Cl$_2$ gave an Ir(II)–Ir(II) species with

(18) (a) Rice, S. F.; Gray, H. B. *J. Am. Chem. Soc.* **1981**, *103*, 1593. (b) Dallinger, R. F.; Miskowski, V. M.; Gray, H. B.; Woodruff, W. H. *J. Am. Chem. Soc.* **1981**, *103*, 1595.

(19) (a) Coleman, A. W.; Eadie, D. T.; Stobart, S. R. *J. Am. Chem. Soc.* **1982**, *104*, 922. (b) Bushnell, G. W.; Fjeldsted, D. O. K.; Stobart, S. R.; Zaworotko, M. J. *J. Chem. Soc., Chem. Commun.* **1983**, 580.

(20) (a) Beveridge, K. A.; Bushnell, G. W.; Dixon, K. R.; Eadie, D. T.; Stobart, S. R. *J. Am. Chem. Soc.* **1982**, *104*, 920. (b) Atwood, J. L.; Beveridge, K. A.; Bushnell, G. W.; Dixon, K. R.; Eadie, D. T.; Stobart, S. R.; Zaworotko, M. J. *Inorg. Chem.* **1984**, *23*, 4050.

a greater M–M contraction (3.163 to 2.737 Å) and a substantial decrease in the dihedral angle (73.1[21] to 51.6°). In contrast to the ground state of $[Ir(COD)(\mu\text{-pz})]_2$, the ground-state geometry of the hydroxypyridinate complexes is already twisted by 25° away from a eclipsed conformation. The more nearly staggered conformation lessens repulsion of the COD ligands and allows larger decreases in the M–M separation and the dihedral angle of the excited state. Less rigidity leads to a larger Stokes shift.

The steric control of excited state rigidity affects the values of the temperature-independent rate constants that describe the deactivation of the excited state. The slightly larger values of k_{nr} (temperature-independent nonradiative deactivation rate constants) for the hydroxypyridinate complexes are consistent with their lower emission energies (Table II) and the higher degree of distortion between the excited and ground states. The expression for the transition probability of nonradiative decay by vibrational relaxation, as derived by Engleman and Jortner[22] is of interest here. In the low-temperature, weak-coupling limit, the transition probability, W (proportional to k_{nr}), is approximated by eq 8 where

$$W = \left(\frac{C^2}{\hbar}\right)\left(\frac{2}{\hbar\omega_M \Delta E}\right)^{1/2}\left(\exp\frac{(-\gamma \Delta E)}{\hbar\omega_M}\right) \quad (8)$$

ΔE is the energy difference between ground and excited states, ω_M is the frequency of the deactivating vibration(s), C is the electronic coupling matrix element, and γ is an expression related to the displacement of equilibrium geometries between the ground and excited states. Thus, if the deactivation modes and C terms are approximately the same for a given set of compounds, k_{nr} decreases exponentially with $\gamma\Delta E$.[23,24] In the hydroxypyridinate complexes, the decrease in ΔE is partially offset by the increase in γ caused by the increased excited-state distortion.

In a similar spirit, the smaller radiative rate constants (k_r) for the hydroxypyridinate complexes in comparison with those of $[Ir(COD)(\mu\text{-pz})]_2$ can also be rationalized. The Strickler–Berg equation[10] approximates the magnitude of k_r (eq 9), where n is

$$k_r = 2.88 \times 10^{-9}(n^2)\langle\bar{\nu}^3\rangle^{-1}(g_1/g_2)\int \epsilon \, d \ln \bar{\nu} \quad (9)$$

the refractive index of the medium, g_1 and g_2 are the degeneracies of the ground and excited states, respectively, $\langle\bar{\nu}\rangle$ can be approximated by the emission energy maximum, and the integral is proportional to the oscillator strength of the absorption. Thus, k_r increases with the cube of the emission energy and is predicted to be significantly smaller for $[Ir(COD)(\mu\text{-hp})]_2$ and $[Ir(COD)(\mu\text{-mhp})]_2$ than for $[Ir(COD)(\mu\text{-pz})]_2$ because the pz complex emission is higher in energy.

The interpretation of variations in the temperature-dependent deactivation rate constant, k_{nr}, is more difficult because the observed rate may be a composite of several processes. The temperature dependent deactivation of the lowest triplet excited state in face-to-face d^8–d^8 complexes has been suggested[14] to be due to the thermal population of a nonemissive, low-energy ligand field state (labelled ^{3}LF in the Jablonski diagram shown in Figure 8). A possible kinetic scheme for the thermal deactivation process is shown in eq 10 and 11. Application of the steady state ap-

$$^3B \underset{k_{-1}}{\overset{k_1}{\rightleftharpoons}} {}^3LF \quad (10)$$

$$^3LF \xrightarrow{k_2} {}^1A \quad (11)$$

proximation to $[^3LF]$ leads to the expression given in eq 12 for $k_{nr'}$. Two limiting cases are available. In the first case, the

$$k_{nr'} = k_2\frac{k_1}{k_{-1} + k_2} \quad (12)$$

deactivation of ^{3}LF is much faster than repopulation of ^{3}B, ($k_2 \gg k_{-1}$), and $k_{nr'} = k_1$. The Arrhenius parameter (E_a) is the activation barrier between ^{3}B and ^{3}LF and is at least as large the energy difference between the two states. The entropy of activation (A factor) includes contributions due to complex and solvent reorganization and is expected to be near the vibrational limit. In the second limiting case, repopulation of ^{3}B is more rapid than nonradiative decay of ^{3}LF, and $k_{nr'} = k_2(k_1/k_{-1})$. The observed thermal deactivation rate constant includes the equilibrium constant for the formation of ^{3}LF from ^{3}B, and the interpretation of the Arrhenius parameters is less straightforward. The data are not sufficient to determine which limit applies to the compounds studied here; but following the suggestion that a large Arrhenius preexponential factor (i.e. close to the vibrational limit) implies that case 1 is more likely,[24] we assume case 1 for the hydroxypyridinate compounds.

We then explain the significantly smaller activation energies observed for the production of ^{3}LF in $[Ir(COD)(\mu\text{-mhp})]_2$ and $[Ir(COD)(\mu\text{-hp})]_2$ compared to $[Ir(COD)(\mu\text{-pz})]_2$ in the same solvent on the basis of the relative energies of the vibrationally relaxed ^{3}LF and ^{3}B states in the two types of complexes. ^{3}LF for the pz compound will lie higher in energy for three reasons. First, because N-bound ligands are generally higher in the spectrochemical series than O-bound ligands,[25] the pyrazolyl ligand, with two ligating N atoms, has a higher ligand field strength than hydroxypyridinate, which has one N and one O ligating atom. Secondly, the pyrazolyl ligand is a better π-acceptor (and therefore a stronger field ligand) than hydroxypyridinates because both ligating atoms are directly involved in the ligand's aromatic system. Finally, the previously suggested[14] pseudotetrahedral distortion of the ^{3}LF state is expected to be of lower energy in the hydroxypyridinate complexes, as the eight-membered $(IrNCO)_2$ ring allows more flexibility than the analogous six-membered ring in $[Ir(COD)(\mu\text{-pz})]_2$.

At this point we observe that another generalized thermal deactivation mechanism for electronically excited states has been advanced.[10] In this mechanism, the lowest triplet undergoes a thermally activated distortion, which relaxes directly into highly excited vibrational levels of the ground electronic state. We think this mechanism is only subtly different from the LF pathway above and cannot be distinguished on the basis of our kinetic data. Other preliminary experiments suggest the ^{3}LF state is involved in the temperature dependent deactivation of the ^{3}B state. Variation of the ligand field with constant geometric restraints was achieved through comparison of the Rh_2 complexes with the corresponding Ir_2 complexes. Excitation of the d–p band of $[Rh(COD)(\mu\text{-hp})]_2$ in MTHF yields a weak emission at ca. 460 nm. At 77 K, a very weak shoulder appears at ca. 570 nm. In contrast to the spectra of the Ir_2 compounds, the Rh_2 compounds exhibit phosphorescence[26] that is much weaker than the fluorescence. We attribute the very small phosphorescence quantum yield of $[Rh(COD)(\mu\text{-hp})]_2$ to the expected lower energy gap between ^{3}LF and ^{3}B in the Rh complexes. Further experiments in this area are in progress.

Comparison of Excited-State Reactivity. As previously reported, visible-light irradiation of $[Ir(COD)(\mu\text{-hp})]_2$ in CH_2Cl_2 and DCE results in no reaction, while irradiation in $CDCl_3$ (NMR tube) or in CCl_4 yields a net oxidation reaction.[1] The CCl_4 reaction gives mononuclear $[Ir(COD)(hp)Cl_2]$ in ca. 85% yield (by ^{1}H NMR). This reaction is the result of the formal four-electron oxidation of $[Ir(COD)(\mu\text{-hp})]_2$ to give 2 equiv of a mononuclear Ir(III) complex that we characterized by X-ray crystallography. We believe that the initial step of the reaction is similar to the one proposed by Gray et al. for $[Ir(COD)(\mu\text{-pz})]_2$ photooxidation chemistry. The irradiation of $[Ir(COD)(\mu\text{-pz})]_2$ in CH_2Cl_2 or

(21) Two different solvates of $[Ir(CO)(PPh_3)(\mu\text{-pz})]_2$ have been characterized crystallographically,[20b] with slightly different Ir–Ir distances and dihedral angles. Average values are quoted here.
(22) Engleman, R.; Jortner, J. *Mol. Phys.* **1970**, *18*, 145.
(23) Caspar, J. V.; Kober, E. M.; Sullivan, B. P.; Meyer, T. J. *J. Am. Chem. Soc.* **1982**, *104*, 630.
(24) Caspar, J. V.; Meyer, T. J. *J. Am. Chem. Soc.* **1983**, *105*, 5583.
(25) Cotton, F. A.; Wilkinson, G. W. *Advanced Inorganic Chemistry*, 4th ed.; Wiley: New York, 1980.
(26) Rodman, G. Ph.D. Thesis, 1987.

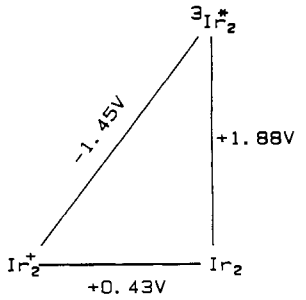

Figure 10. Modified Latimer diagram for the one-electron chemistry of [Ir(COD)(μ-hp)]$_2$ in CH_2Cl_2 constructed to follow the convention of ref 7.

Table VII

halocarbon	$E_{p/2}$,[a] V vs SSCE	halocarbon	$E_{p/2}$,[a] V vs SSCE
CCl_4	−1.33	CH_2Cl_2	−2.44
$CHCl_3$	−1.90	CH_3Cl	−2.76

[a] Half-peak potential from linear sweep chronoamperometry, taken from ref 32.

in dichloroethane (DCE) yields the two-center oxidative-addition products [Ir(COD)(μ-pz)]$_2$($ClCH_2$)(Cl), and [Ir(COD)(μ-pz)Cl]$_2$, respectively.[27] These reactions of [Ir(COD)(μ-pz)]$_2$ proceed through the $^3B_2$ state.[11]

The similarities we have observed in the photophysics of [Ir(COD)(μ-hp)]$_2$ and [Ir(COD)(μ-pz)]$_2$ suggest that the [Ir(COD)(μ-hp)]$_2$ photoreaction also proceeds through the ^3B excited state. From the ground-state reduction potential for the one-electron oxidation of [Ir(COD)(μ-hp)]$_2$ of 0.43 V[28] and the 0–0 energy of the ^3B state (approximated by the onset of the phosphorescence band), a modified Latimer diagram[28] similar to the [Ir(COD)(μ-pz)]$_2$ diagram was constructed for [Ir(COD)(μ-hp)]$_2$ (Figure 10 where $^3Ir_2^*$ represents the ^3B excited state of [Ir(COD)(μ-hp)]$_2$). Although the excited-state reduction potential ($Ir_2^+/^3Ir_2^*$ = −1.45 V) for [Ir(COD)(μ-hp)]$_2$ is slightly less negative than the −1.63V reported for [Ir(COD)(μ-pz)]$_2$,[7,29] the failure of the $^3B_2$[Ir(COD)(μ-hp)]$_2$ excited state to reduce CH_2Cl_2 and DCE cannot be rationalized on this basis.[31] If this were the case, applicable electron-transfer theory predicts that differences in CCl_4 and $HCCl_3$ reactivity would also be apparent, even though CH_2Cl_2 and DCE are significantly harder to reduce[32] (Table VII). We have also examined as a potential explanation the more substantial differences between [Ir(COD)(μ-pz)]$_2$ and [Ir(COD)(μ-hp)]$_2$. These are their room-temperature lifetimes of 250 ns[11] for the pz complex versus 0.8 ns for the hp complex. But again the decrease in reactivity is difficult to rationalize because the short lifetime of the ^3B excited state should also preclude reaction with CCl_4 and $HCCl_3$.

These points remain unresolved, but we speculate that large differences in the rates of later steps in the overall chemical reaction (four- vs two-electron chemistry) actually determine the observed differences in net reactivity. For example, the one-electron-transfer quenching of the shortlived ^3B [Ir(COD)(μ-hp)]$_2$ excited state is fast in all the neat halocarbons, but a succeeding step (i.e. the second electron transfer, decomposition of an organic radical anion etc.) is slow so that back-electron-transfer is competitive. Our data are insufficient to enable us to answer this question, but electrochemical experiments that address the reactivity differences between the [Ir(COD)(μ-hp)]$_2^+$ and [Ir(COD)(μ-pz)]$_2^+$ radical cations are in progress and may support or refute this hypothesis.

Acknowledgment. We wish to thank Dr. David Boyd for valuable discussions and Johnson Matthey, Inc., for a loan of rhodium and iridium trichloride.

Supplementary Material Available: Derivation of an excited state deactivation model (Appendix) and tables of quantum yield and lifetime data as a function of temperature for [Ir(COD)(μ-L)]$_2$ complexes (5 pages). Ordering information is given on any current masthead page.

(27) Caspar, J. V.; Gray, H. B. *J. Am. Chem. Soc.* **1984**, *106*, 3029.
(28) Boyd, D. C. Ph.D. Thesis, University of Minnesota, 1987.
(29) Boyd, D. C.; Rodman, G. S.; Mann, K. R. *J. Am. Chem. Soc.* **1986**, *108*, 1779.
(30) Scandola, F.; Balzani, V.; Schuster, G. B. *J. Am. Chem. Soc.* **1981**, *103*, 2519.
(31) To clarify this argument, consider the photoreaction of [Ir(COD)(μ-pz)]$_2$ with DCE. From the experimentally determined[7] lifetime of the $^3B_2$ state in the absence of DCE and the quenching rate constant of DCE (7.3×10^5 M^{-1} s^{-1}), an upper limit for the quantum yield of the photoreaction is calculated to be 0.7 (pure DCE is 12 M). Experimentally, the quantum yield was determined to be 0.047 ± 0.004, meaning that less than 10% of the quenched species react to form the photoproduct. A similar calculation for [Ir(COD)(μ-hp)]$_2$ gives 0.007 for the *upper limit* of the reaction quantum yield of the ^3B state with DCE. Thus, even if the excited state potential were the same as the ^3B state of [Ir(COD)(μ-pz)]$_2$, the reaction of the ^3B state of [Ir(COD)(μ-hp)]$_2$ with DCE might be expected to proceed, but 100 times more slowly. In fact, no detectable reaction is observed over several hours, although prolonged (several days) irradiation led to some decomposition of the complex. A study of the ability of various halogenated solvents to quench the ^3B state of [Ir(COD)(μ-hp)]$_2$ would in principle be useful in understanding the photoredox behavior of the complex.
(32) Meites, L.; Zuman, P.; Rupp, E. B. *CRC Handbook Series in Organic Electrochemistry*; CRC: West Palm Beach, FL, 1977; Vol. III.
(33) See paragraph at end of paper regarding supplementary material.